International Journal on Recent and Innovation Trends in Computing and Communication
ISSN: 2321-8169 Volume: 11 Issue: 11
Article Received: *25 July 2023* ***Revised:*** *12 September 2023* ***Accepted:*** *30 September 2023*

Electrical Properties of CUO-Embedded PPY Composite Samples

Promila Jangra*, Vikram Singh
Dept of Physics, OSGU, Hisar Corresponding Author*

Abstract: In the current study, three distinct CuO doping doses were used to create pure and CuO nanoparticle-doped polypyrrole-based samples by a straightforward chemistry-based polymerization procedure. A variety of methods were employed to characterize the prepared samples. The prepared samples' X-ray diffraction spectra show that they are quasi-crystals in nature. These samples' Fourier transformation infrared spectroscopy shows the different necessary fundamental bands, confirming the synthesis of the anticipated samples. The morphology of the synthesized samples can be seen in the field emission scanning electron microscopy. Using thermal gravimetric analysis, the thermal characteristics of the prepared samples were examined. Additionally, the electrical characteristics of the manufactured samples were examined between 293 and 393 K in temperature. As the temperature rises, the conductivity of the produced samplesincreases, indicating that they are semi-conducting.

Keywords: *PPY; CuO; TGA; Semi-conductor; Mott's Hopping.*

Introduction

Insulators comprise most of the polymers reported in the literature. Subsequent studies, however, showed that polymers can act like semiconducting materials. Polymers possess unique optical, electrical, and thermal properties that make them potentially useful in a wide range of fields. Polypyrrole (PPY) has garnered significant interest owing to its non-redox doping, robust thermal and environmental stability, elevated conductivity, and feasibility, alongside other conducting polymers. When expressed as a composite, the properties of PPY change significantly.

These composites have shown promise in applications such as electrochromic displays, temperature and current sensor devices, polymeric batteries, and shielding at the electromagnetic/radio frequency interface in electronic equipment, such as the plastic casing of computers and cell phones. To further improve PPY's mechanical qualities, conductivity, and processability, metal oxides (MOs) can be combined with it. Making PPY-MO composites is challenging because it is hard to achieve chemical interactions between PPY and MOs. Researchers are still focused on creating MO and PPY composites using a range of methods due to their improved properties and potential applications in multiple fields [1]. In order to create a variety of nanocomposite materials, conducting polymers have up until now been utilised as a shell around inorganic nanoparticles such as CuO [2]. By employing ultrasonic irradiation, Xia and Wang [3] produced a PPY/CuO nanocomposite. Schnitzler and Zarbin [4] synthesised hybrid materials, such as CuO nanoparticles and PPY, by using the sol-gel technique. Transition-metal oxides are the most often used cathode candidates in the development of lithium and lithium-ion battery technologies [5].

Other crystalline oxides have also been used as cathodes in solar cells [6,7] and rechargeable lithium batteries [8,9], including V_2O_5, MnO_2, MoO_3, and WO_3. Furthermore, dielectric/magnetic and electrical properties are combined in PPY filled with materials such as carbonaceous fillers, magnetic particles, or dielectric particles [10–19]. These composites have demonstrated uses in the areas of corrosion management [20], supercapacitors [21], and microwave absorption [22]. Song and colleagues chemically synthesized PPY and NiO composites in the presence of sodium dodecyl benzenesulfonate to form PPY/NiO nanoparticles, nanobelts, and nanotubes. The composite materials' conductivity and thermostability both increased [23–25].The majority of researchers are still focused on the synthesis and characterization of PPY/CuO composites, despite the fact that several investigations into these materials have been reported. However, as far as the author is aware, no publication has been done on the investigation of dynamical parameters for PPY/CuO composites using techniques such as TGA. Consequently, a comprehensive study utilizing different CuO concentrations in PPY and techniques is needed.

Experimental DetailsSample Preparation

Chemical oxidative polymerization synthesis was used to create the pure PPY and PPY/CuO composite samples. To

International Journal on Recent and Innovation Trends in Computing and Communication
ISSN: 2321-8169 Volume: 11 Issue: 11
Article Received: *25 July 2023* ***Revised:*** *12 September 2023* ***Accepted:*** *30 September 2023*

do this, separate aqueous solutions of ferric chloride and pyrrole at molar concentrations of 1.25 M and 1 M were produced. After that, the produced solutions werechilled for two hours in a refrigerator.

After that, an ice bath was used to keep the monomer solution at a temperature of between 0 and 4 ºC. Following the dropwise addition of the oxidant solution to the monomer solution, the polymerization reaction swiftly begins, and it is allowed toreact for 24 hours. Following the proper amount of time, the solution is allowed to filter through filter paper. The resulting yield is then rinsed with 1 M HCl and acetone until the filtrate is colorless. This yield was then vacuum-dried after being air-dried first. A pestle and mortar were used to smash the dry sample into a fine powder. The 5, 10, and 15% weight percentage CuO doped PPY composite materials were synthesized in a similar manner.

Experimental Techniques

XRD patterns with CuKα in the angle of 2θ (10-80º) were recorded using the Rigaku Miniflex-II diffractometer at a slow scanning rate of 2º/min. X-ray diffraction (XRD) data was utilized to determine the crystal structure of the samples. When utilizing a Shimadzu IR affinity-1 8000 FTIR spectrophotometer for the FTIR analysis, the powder sample was combined with dry KBr at a weight ratio of 1:20.

Utilizing the EVO 18 scanning electron microscope, the microstructure of the surface was investigated. Thermogravimetric analysis was performed using a TA apparatus (model number SDT Q600) heated at 10 ºC/min in a nitrogen atmosphere. We tested DC conductivity at 1V and temperatures between 25 and 120 ºC, with a 2 ºC fluctuation, using the Keithley 6517B electrometer.

Results and Discussion

X-ray Diffraction (XRD) Analysis

The XRD patterns of PPY and PPY/CuO composites are shown in Figure 1. The PPY and PPY/CuO composite samples' XRD patterns show two identical peaks at around 21.44 and 26.12 degrees, while a soldier is located at approximately 16.10 degrees. When CuO nanoparticles are added to PPY symmetry, the strength of the peaks changes considerably, indicating a strong interaction between CuO and PPY. The presence of quinoid and benzenoid rings in both perpendicular and parallel orientations accounts for these two beaks. Furthermore, the existence of these two peaks suggests that the processed samples have quasi-crystal structure.

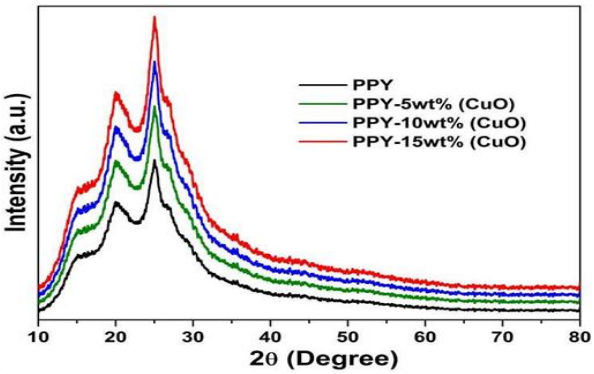

Figure 1: XRD patterns of PPY and PPY/CuO composites.

Fourier Transform Infrared (FTIR) Analysis

Figure 2 displays the FTIR spectra of the pure and CuO-doped PPY composite samples. Distinct vibrations between 400 and 2000 cm^{-1} are visible in the FTIR spectra. It displays distinct bands at518, 813, 1159, 1321, 1493, and 1591 cm^{-1}. Para-disubstituted aromatic rings and C-H out-of- plane bending vibration are responsible for the bands at 518 and 813 cm^{-1}, respectively. An apparent band around 1321 cm^{-1} represents the C-N stretching vibrations. When the plane is curved, vibration in C-H occurs at 1159 cm^{-1} [26]. The bands observed in the 1450-1600 cm^{-1} region are believed to be caused by non-symmetric C6 ring stretching modes [27]. The benzenoid ring units are visible in the lower frequency mode at 1493 cm^{-1}, but the quinoid rings are importantin the higher frequency vibration at 1591 cm^{-1}. The peak observed at 2300 cm^{-1} is caused by aromatic C-H stretching vibrations, whereas the band observed in the range 2950-3300 cm^{-1} is attributed to N-H stretching of aromatic amines [28–30].

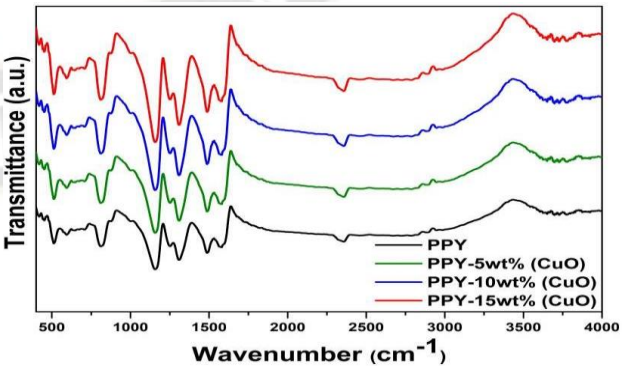

Figure 2: FTIR spectra of PPY and PPY/CuO composites

Field Emission Scanning Electron Microscopy (FESEM)

Typical FESEM images for pure PPY and PPY/CuO composite samples are shown in Figure 3(a-d). The current

International Journal on Recent and Innovation Trends in Computing and Communication
ISSN: 2321-8169 Volume: 11 Issue: 11
Article Received: *25 July 2023* ***Revised:*** *12 September 2023* ***Accepted:*** *30 September 2023*

samples' FESEM photos show that their particles have the same morphology as clean and CuO-doped PPY samples. No CuO nanoparticles are seen in the FESEMpictures of the composite samples, which may be because the CuO nanoparticles have been incorporated into the PPY matrix. In this case, PPY acts as the shell and CuO nanoparticles as the core [31].

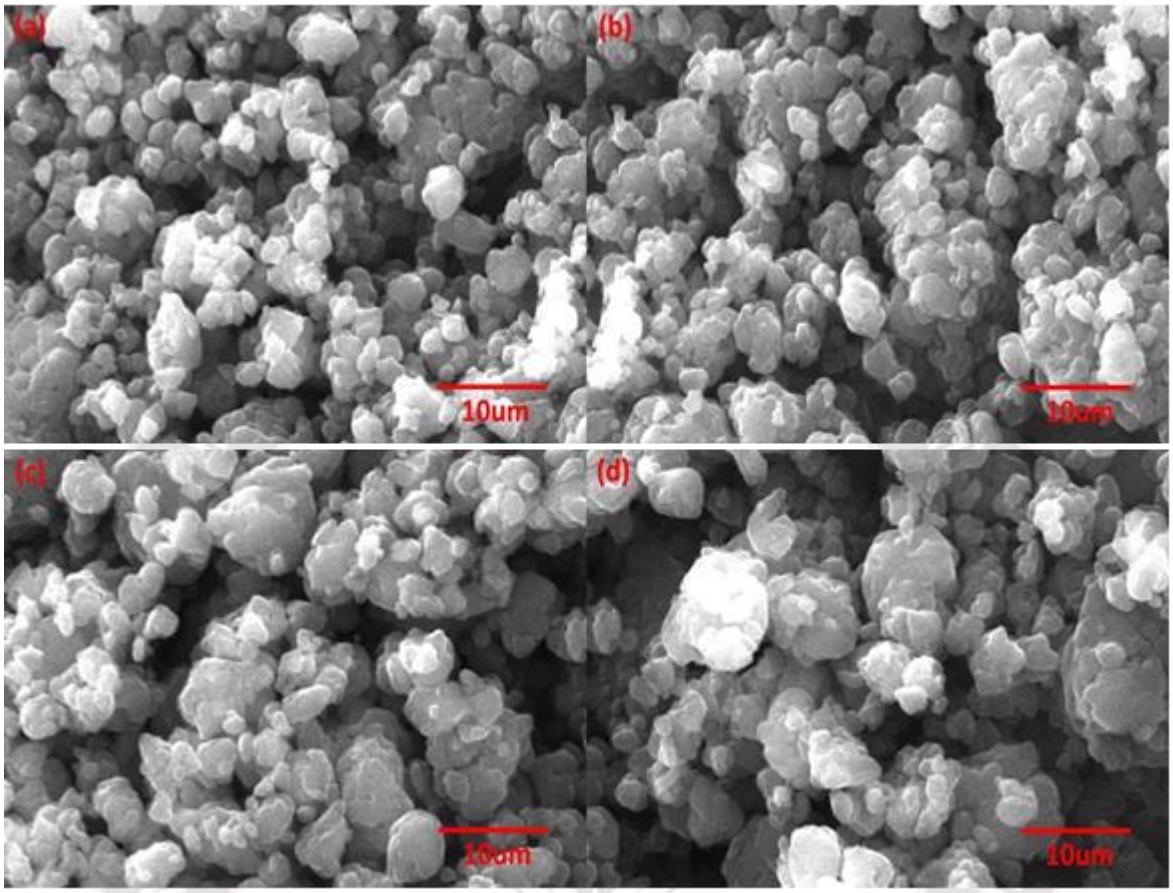

Figure 3: FESEM images of PPY and PPY/CuO composites

Thermogravimetric Analysis (TGA)

TGA thermograms of PPY and PPY/CuO composites in a nitrogen environment are shown in Figure 4.

The TGA study of PPY and PPY/CuO composites reveals the four mechanisms of weightreduction.

1. It is believed that the first stage of dehydration starts at about 100 ºC and is brought on by water that has been absorbed at the doped polymer's surface desorbing [32].
2. The second step happens at around 250 ºC as a result of the protonic acid component beingeliminated [32].
3. The polymer chain breaks at around 510 °C for the third and 640 °C for the fourth, potentially leading to the generation of gases [33].

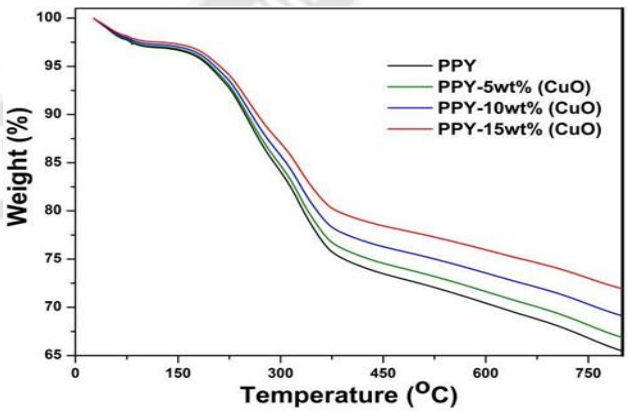

Figure 4: TGA thermograms of PPY and PPY/CuO composites

Current-Voltage (I-V) Characteristics (DC Conductivity)

Because the current in conducting polymers does not increase linearly with applied voltage, their conduction

International Journal on Recent and Innovation Trends in Computing and Communication
ISSN: 2321-8169 Volume: 11 Issue: 11
Article Received: *25 July 2023* ***Revised:*** *12 September 2023* ***Accepted:*** *30 September 2023*

mechanisms are very different from those of intrinsic semiconductors [34–36]. When negative and positive charges are added to conducting polymers, the rigid conduction or valence bands do not fill right away. In conductive polymers, there are no permanent dipoles. Actually, there are sporadic charge (polaron) trapping sites in the sample. When an external field is applied, strong coupling between electrons and phonons causes lattice distortions around the doped charge. As a result, their confined motion functions as an effective electric dipole and charge trapping intensifies. Quasiparticles such as bipolarons and polarons are so produced. This time, charge is carried by these polarons and bipolarons. A nonlinear curve is produced and the increase in current relative to voltage is accelerated by the formation of polarons and bipolarons, which increases withincreasing applied field [37]. Within the temperature range of 293 to 393 K, the electrical characteristics of the prepared samples were examined. The fluctuation in electrical conductivity with temperature is shown in Figures 5(a,b).

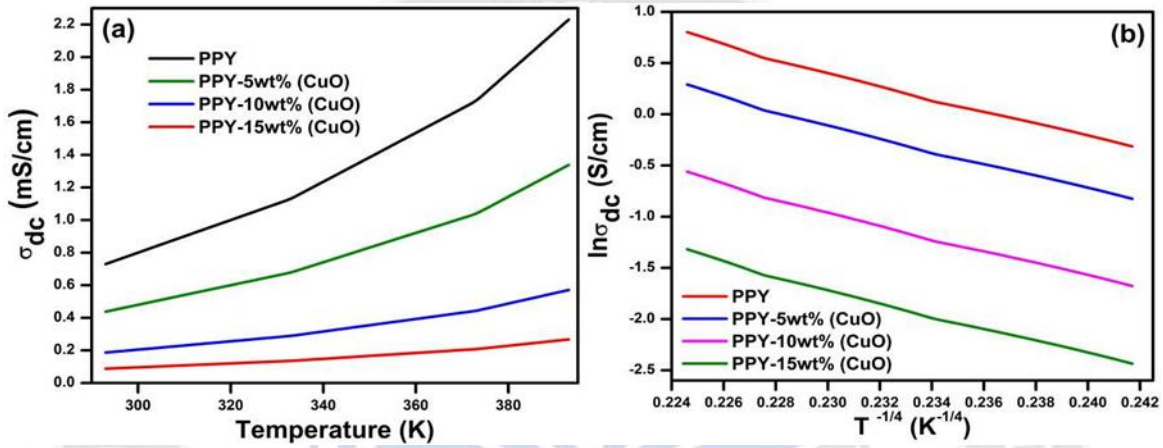

Figure 5: (a) Variation in electrical properties and (b) ln dc vs $T^{-1/4}$ of PPY and PPY/CuO composites

Based on the observed I-V characteristics of these samples, equation (1), which is given as, has been utilized to determine the values of dc electrical conductivities (dc) at different temperatures at 1V [38–40].

$$\sigma_{dc} = \frac{I \times L}{V \times A} \quad (1)$$

where V denotes voltage and L and A, respectively, denote the sample's thickness and area.The dc conductivity variation with temperature for PPY and PPY/CuO composites is also shown in Figure 5a. It was discovered that every sample's DC conductivity (dc) measurement followed the Arrhenius relation, which is represented by equation 2, which is [41–44].

$$\sigma_{dc}(T) = \sigma_0 \exp\left(\frac{-W}{kT}\right) \quad (2)$$

Where W is the thermal activation energy of electrical conduction, k is Boltzmann's constant, and σ0 is the pre-exponential parameter that depends on semiconductor nature.

Equation 2 can be used to calculate the activation energy due to electrical conduction based on the slope of the curve ln dc versus $T^{-1/4}$. The slope of each sample is found by linear fitting; the pristine PPY sample has an activation energy of 5.54, 4.45, 3.76, and 3.01 meV, while the CuO- doped PPY sample has values of 5, 10, and 15 weight percent. These activation energy values show that the activation energy values drop as the doping concentration increases, indicating thatless energy is needed for the charge transport mechanism [45–47].

A similar extremely strong linear fitting (with linearity 0.99) is seen in Figure 5b, which plots $\ln\sigma^{dc}$ vs. $T^{-1/4}$. It demonstrates that all of the samples show three-dimensional (3D) charge transport, which was previously explained by equation (3) [48–50].

$$\sigma_{dc} = \sigma_0 e^{-\left(\frac{T_0}{T}\right)^{\gamma}} \quad (3)$$

Where To is the Mott's characteristic temperature associated with the electronic wave function's degree of localization. The exponent = 1/(1+d) determines the dimensionality of the conducting media. The Mott's model was introduced to explain the variable range hopping (VRH) of disordered materials in the low temperature zone. Nonetheless, for the currently available composites, this model performs well in

explaining dc conductivity data at high temperatures [51–53].

Conclusions

For the preparation of PPY and CuO-doped PPY composite samples, the chemical oxidative polymerization synthesis method was employed. The FTIR spectra of the generated samples showthe presence of strongly conducting state peaks of quinoid and benzenoid rings, indicating that thematerials are PPY-based pure and composite samples in the emerald salt form. The quasi-crystal nature of the currently manufactured samples is indicated by their XRD pattern. According to TGA, both the pristine and doped samples retain over 65% of their weight even at temperatures ashigh as 800 ºC. This suggests that as the concentration of CuO nanoparticle doping grows, so does the stability of the produced samples. Particle sizes in the range of 1 to 10 um are indicated by the FESEM pictures of the produced samples. The produced samples' charge transport mechanism isbased on the Mott's variable hopping model.

References

1. Gangopadhyay, R., & De, A. (2000). Conducting polymer nanocomposites: a brief overview. *Chemistry of materials*, *12*(3), 608-622.
2. Li, X., Wang, G., Li, X., & Lu, D. (2004). Surface properties of polyaniline/nano-TiO2 composites. Applied Surface Science, 229(1-4), 395-401.
3. Xia, H., & Wang, Q. (2002). Ultrasonic irradiation: a novel approach to prepare conductive polyaniline/nanocrystalline titanium oxide composites. *Chemistry of Materials*, *14*(5), 2158-2165.
4. Schnitzler, D. C., & Zarbin, A. J. (2004). Organic/inorganic hybrid materials formed from TiO2 nanoparticles and polyaniline. *Journal of the Brazilian Chemical Society*, *15*, 378- 384.
5. Nagaura, T., & Tazawa, K. (1991). Prog. Batteries Sol. Cells 9, 20 (1990), JR Dahn, U, Von Sacken, MR Jukow, and H. Al-Janaby. *J. Etelectrochern. Soc*, *137*, 2207.
6. Yoneyama, H., Kishimoto, A., & Kuwabata, S. (1991). Charge–discharge properties of polypyrrole films containing manganese dioxide particles. *Journal of the Chemical Society, Chemical Communications*, (15), 986-987.
7. Gemeay, A. H., Nishiyama, H., Kuwabata, S., & Yoneyama, H. (1995). Chemical preparation of manganese dioxide/polypyrrole composites and their use as cathode active materials for rechargeable lithium batteries. *Journal of the Electrochemical Society*, *142*(12), 4190.
8. Li, G., Chu, C. W., Shrotriya, V., Huang, J., & Yang, Y. (2006). Efficient inverted polymer solar cells. *Applied physics letters*, *88*(25).
9. Shrotriya, V., Li, G., Yao, Y., Chu, C. W., & Yang, Y. (2006). Transition metal oxides asthe buffer layer for polymer photovoltaic cells. *Applied Physics Letters*, *88*(7).
10. Saini, P., Choudhary, V., Vijayan, N., & Kotnala, R. K. (2012). Improved electromagnetic interference shielding response of poly (aniline)-coated fabrics containing dielectric and magnetic nanoparticles. *The Journal of Physical Chemistry C*, *116*(24), 13403-13412.
11. Zhang, B., Du, Y., Zhang, P., Zhao, H., Kang, L., Han, X., & Xu, P. (2013). Microwave absorption enhancement of Fe3O4/polyaniline core/shell hybrid microspheres with controlled shell thickness. *Journal of Applied Polymer Science*, *130*(3), 1909-1916.
12. Abbas, S. M., Chatterjee, R., Dixit, A. K., Kumar, A. V. R., & Goel, T. C. (2007). Electromagnetic and microwave absorption properties of (Co2+–Si4+) substituted barium hexaferrites and its polymer composite. *Journal of applied physics*, *101*(7).
13. Jumali, M. H., Izzuddin, I., Ramli, N., Salleh, M., & Yahaya, M. (2009). Comparative studies on microstructural and gas sensing performance of TiO2 and TiO2-PANi nanocomposite thin films. *Solid State Sci. Technol*, *17*, 126-131.
14. Saini, P., Arora, M., Gupta, G., Gupta, B. K., Singh, V. N., & Choudhary, V. (2013). High permittivity polyaniline–barium titanate nanocomposites with excellent electromagnetic interference shielding response. *Nanoscale*, *5*(10), 4330-4336.
15. Ganesan, R., & Gedanken, A. (2008). Organic–inorganic hybrid materials based on polyaniline/TiO2 nanocomposites for ascorbic acid fuel cell systems. *Nanotechnology*, *19*(43), 435709.
16. Pawar, S. G., Patil, S. L., Chougule, M. A., Raut, B. T., Jundale, D. M., & Patil, V. B. (2010). Polyaniline: TiO2 nanocomposites: Synthesis and characterization. *Arch. Appl. Sci. Res*, *2*(2), 194-201.
17. Dey, A., De, S., De, A., & De, S. K. (2004). Characterization and dielectric properties of polyaniline–TiO2 nanocomposites. *Nanotechnology*, *15*(9), 1277.
18. Maiti, S., Shrivastava, N. K., Suin, S., & Khatua, B. B. (2013). Polystyrene/MWCNT/graphite nanoplate nanocomposites: efficient electromagnetic interference shielding material through graphite nanoplate–MWCNT–graphite nanoplate networking. *ACS Applied Materials & Interfaces*, *5*(11), 4712-4724.
19. Saini, P., & Choudhary, V. (2013). Enhanced

electromagnetic interference shielding effectiveness of polyaniline functionalized carbon nanotubes filled polystyrene composites. *Journal of nanoparticle research*, *15*, 1-7.

20. Saini, P., Choudhary, V., Singh, B. P., Mathur, R. B., & Dhawan, S. K. (2011). Enhanced microwave absorption behavior of polyaniline-CNT/polystyrene blend in 12.4–18.0 GHz range. *Synthetic Metals*, *161*(15-16), 1522-1526.
21. D. A. Brown, D. Cunningham and W. K. Glass, *Spectrochim. Acta* **23 (**2012) 343.
22. Jeyaprabha, C., Sathiyanarayanan, S., & Venkatachari, G. (2006). Polyaniline as corrosion inhibitor for iron in acid solutions. *Journal of applied polymer science*, *101*(4), 2144-2153.
23. Song, G., Bo, J., & Guo, R. (2005). Synthesis of the composite material of polyaniline/NiO/sodium dodecylbenzenesulfonate in micelles. Colloid and Polymer Science, 283, 677-680.
24. Song, G., Han, J., & Guo, R. (2007). Synthesis of polyaniline/NiO nanobelts by a self- assembly process. *Synthetic Metals*, *157*(4-5), 170-175.
25. Han, J., Song, G., & Guo, R. (2006). Synthesis of rectangular tubes of polyaniline/NiO composites. *Journal of Polymer Science Part A: Polymer Chemistry*, *44*(13), 4229-4234.
26. Su, S. J., & Kuramoto, N. (2000). Processable polyaniline–titanium dioxide nanocomposites: effect of titanium dioxide on the conductivity. *Synthetic metals*, *114*(2), 147-153.
27. Oey, C. C., Djurišić, A. B., Wang, H., Man, K. K. Y., Chan, W. K., Xie, M. H., ... & Chui, P. C. (2006). Polymer–TiO2 solar cells: TiO2 interconnected network for improved cell performance. *Nanotechnology*, *17*(3), 706.
28. Raghavendra, S. C., Khasim, S., Revanasiddappa, M., Ambika Prasad, M. V. N., & Kulkarni, A. B. (2003). Synthesis, characterization and low frequency ac conduction of polyaniline/fly ash composites. *Bulletin of Materials Science*, *26*, 733-739..
29. Chen, W., Li, X., Xue, G., Wang, Z., & Zou, W. (2003). Magnetic and conducting particles: preparation of polypyrrole layer on Fe3O4 nanospheres. *Applied surface science*, *218*(1- 4), 216-222.
30. Klug, H. P., & Alexander, L. E. (1974). *X-ray diffraction procedures: for polycrystalline and amorphous materials* (p. 992).
31. Chen, S. A., Chuang, K. R., Chao, C. I., & Lee, H. T. (1996). White-light emission from electroluminescence diode with polyaniline as the emitting layer. *Synthetic Metals*, *82*(3),207-210.
32. Dumitrescu, I., Nicolae, C. A., Mocioiu, A. M., Gabor, R. A., Grigorescu, M., & Mihailescu, M. (2009). Synthesis and characterization of conductive polymers with enhanced solubility. *UPB Sci Bull, Ser A*, *71*, 63-72.
33. Kalsi, P. C., Mudher, K. S., Pandey, A. K., & Iyer, R. H. (1995). Thermal studies on unirradiated and γ-irradiated polymer of allyl diglycol carbonate. *Thermochimica acta*, *254*, 331-336.
34. Anslyn, E. V., & Dougherty, D. A. (2006). *Modern physical organic chemistry*. Universityscience books.
35. Gupta, R., Kumar, V., Goyal, P. K., Goyal, S. L., Kandwal, P., Mohapatra, P. K., & Rajeswari, B. (2011). Effect of γ-irradiation on thermal stability of CR-39 polymer. *Adv. Appl. Sci. Res.*, *2*, 248-254.
36. Reghu, M., Cao, Y., Moses, D., & Heeger, A. J. (1993). Counterion-induced processibility of polyaniline: Transport at the metal-insulator boundary. *Physical Review B*, *47*(4), 1758.
37. Earle, M. D. (1942). The electrical conductivity of titanium dioxide. *Physical Review*, *61*(1-2), 56.
38. Machappa, T., & Prasad, M. A. (2009). AC conductivity and dielectric behavior of polyaniline/sodium metavenadate (PANI/NaVO3) composites. *Physica B: Condensed Matter*, *404*(21), 4168-4172.
39. Anilkumar, K. R., Parveen, A., Badiger, G. R., & Prasad, M. A. (2009). Effect of molybdenum trioxide (MoO3) on the electrical conductivity of polyaniline. *Physica B: Condensed Matter*, *404*(12-13), 1664-1667.
40. Patil, R., Roy, A. S., Anilkumar, K. R., Jadhav, K. M., & Ekhelikar, S. (2012). Dielectric relaxation and ac conductivity of polyaniline–zinc ferrite composite. *Composites Part B: Engineering*, *43*(8), 3406-3411.
41. Ozkazanc, E., Zor, S., & Ozkazanc, H. (2012). Synthesis, characterization, and AC conductivity of polyaniline/selenium composites. *Journal of Macromolecular Science, Part B*, *51*(11), 2122-2132.
42. De, S., Dey, A., & De, S. K. (2005). Charge transport mechanism of vanadium pentoxide xerogel-polyaniline nanocomposite. *The European Physical Journal B-Condensed Matterand Complex Systems*, *46*, 355-361.
43. Elliott, S. R. (1987). Ac conduction in amorphous chalcogenide and pnictide semiconductors. *Advances in physics*, *36*(2), 135-217.
44. Punia, R., Kundu, R. S., Dult, M., Murugavel, S., & Kishore, N. (2012). Temperature and frequency dependent conductivity of bismuth zinc vanadate semiconducting glassy system. *Journal of Applied Physics*, *112*(8).
45. Gosh, M., Barman, A., Meikap, A. K., De, S. K., &

Chatterjee, S. (1999). Hopping transport in HCl doped conducting polyaniline. *Physics Letters A*, *260*(1-2), 138-148..

46. Bisquert, J., Garcia-Belmonte, G., Bueno, P., Longo, E., & Bulhoes, L. O. S. (1998). Impedance of constant phase element (CPE)-blocked diffusion in film electrodes. *Journal of Electroanalytical Chemistry*, *452*(2), 229-234.
47. Patil, R., Roy, A. S., Anilkumar, K. R., Jadhav, K. M., & Ekhelikar, S. (2012). Dielectric relaxation and ac conductivity of polyaniline–zinc ferrite composite. *Composites Part B: Engineering*, *43*(8), 3406-3411.
48. Nabid, M. R., Golbabaee, M., Moghaddam, A. B., Dinarvand, R., & Sedghi, R. (2008). Polyaniline/TiO2 nanocomposite: enzymatic synthesis and electrochemical properties. *International journal of electrochemical science*, *3*(10), 1117-1126.
49. Li, J., Cui, M., Lai, Y., Zhang, Z., Lu, H., Fang, J., & Liu, Y. (2010). Investigation of polyaniline co-doped with Zn2+ and H+ as the electrode material for electrochemical supercapacitors. *Synthetic metals*, *160*(11-12), 1228-1233.
50. Li, J., Tang, X., Li, H., Yan, Y., & Zhang, Q. (2010). Synthesis and thermoelectric properties of hydrochloric acid-doped polyaniline. *Synthetic Metals*, *160*(11-12), 1153- 1158.
51. Epstein, A. J., Ginder, J. M., Zuo, F., Bigelow, R. W., Woo, H. S., Tanner, D. B., ... & MacDiarmid, A. G. (1987). Insulator-to-metal transition in polyaniline. *SyntheticMetals*, *18*(1-3), 303-309.
52. Chatterjee, K., Ganguly, S., Kargupta, K., & Banerjee, D. (2011). Bismuth nitrate doped polyaniline–Characterization and properties for thermoelectric application. *Synthetic metals*, *161*(3-4), 275-279.